Sensor coupling in acoustic media using reciprocity

Johan Vos, Guy G. Drijkoningen, and Jacob T. Fokkema
Delft University of Technology, 2600 GA Delft, The Netherlands

(Received 20 July 1998; accepted for publication 31 December 1998)

In this paper the coupling of a sensor to an acoustic medium is discussed. Based on the acoustic reciprocity theorem, an expression is derived for the motion of the sensor as a function of the undisturbed motion of the embedding medium. What is special here is that the sensor *is* the scattering object. The sensor coupling is affected by two factors: the ratio of the density of the sensor and of the embedding medium (ground), and a frequency-dependent factor depending on the geometry of the sensor. © *1999 Acoustical Society of America.* [S0001-4966(99)02204-3]

PACS numbers: 43.38.Ar, 43.20.Tb [SLE]

INTRODUCTION

A sensor is a device that converts a physical quantity to an electric signal. In this article focus is on motion-sensitive and pressure-sensitive sensors. What the sensor is meant to measure is the motion of the medium if the sensor were not there at all. This can never be the case since the measuring device itself is present. When an acoustic wave arrives at a contrasting medium—e.g., a measuring device—a reflected wave will exist. As a consequence, the original acoustic wavefield will be disturbed. Since it is the goal of measuring devices to obtain values for the original acoustic wave field—the wave field that would exist if no device was present—it is important to have an idea about the magnitude and behavior of the disturbing acoustic field. The fact that a device meant for the detection of an acoustic wave field disturbs this wave field exists in general. In this article, focus is given on the specific case of an acoustic device—a pressure or velocity measuring sensor, embedded *in* a medium—e.g., the earth. It must be stressed here that although the examples in this paper are taken from seismological practice, the theoretical results have an impact on many more fields of application, like in nondestructive testing, underwater acoustics, etc. It will be shown here that if true amplitudes for any acoustical application are desired, a correction must be made for the coupling of the sensor to the probing medium, the amount of which is quantified in this paper.

The sensor coupling is defined to be the ratio between the velocity of the sensor (v_{sens}), and the velocity of the medium (v_{med}) in absence of the sensor:

$$C_{\text{SC}}=\frac{v_{\text{sens}}}{v_{\text{med}}}. \tag{1}$$

In the past, different models were used in order to describe the problem of the sensor coupling. This research was started to address the problem of the sensor coupling as used in seismic exploration, where the sensor on land is the geophone. The geophone is an electro-magnetic device, which is put on top of a spike which furnishes the coupling to the ground. In most theoretical studies for geophones, the sensor was simulated by its case only, neglecting the spike. Tan (1987) was the first to notice that the spike is too important to ignore. In this study, the influence of the spike will be examined. In practice, spikes of geophones are made of steel, so in the analysis the sensor is considered to be a rigid, movable object. It must be stressed here that although these problems are taken from a geophysical practice, the results here pertain to a much more general audience of people who concern themselves with coupling problems.

Sensor coupling involves two phenomena: scattering due to the sensor being there, and boundary effects of the sensor due to bad contact between the sensor and the embedding medium. The first problem is called the interaction coupling, denoted by C_I, and the second contact coupling, denoted by C_C. Then the total sensor coupling can be written as:

$$C_{\text{SC}}=\frac{v_{\text{sens},pc}}{v_{\text{med}}}\,\frac{v_{\text{sens}}}{v_{\text{sens},pc}}=C_I C_C. \tag{2}$$

In the case of interaction coupling, no slip or friction can occur, and the particle velocity shows a continuous behavior when approaching the sensor. Because of differences in material properties between the medium and the sensor, material displacement in absence of the sensor is not exactly the same as the sensor displacement. The sensor can be considered to be a contrasting domain in a half-space, e.g., the earth. In practice, however, slip and friction may occur, and the sensor will not exactly follow the motion of the material in the immediate vicinity of the sensor. This effect is separated in the above by the factor C_C. As an extreme case of this situation, the sensor may be in completely loose contact with the medium. In this paper this situation will not be addressed; only the interaction coupling will be considered, where perfect contact between the sensor and the embedding medium is assumed. In this case the disturbance of the wave field, due to the presence of the sensor, has to be investigated.

The paper is built up as follows. First, a homogeneous half-space is considered, and then the effect of a contrasting domain in the half-space is formulated. The special case of a cylindrical sensor will be considered for its analytical convenience: Most of the integrals can be determined analytically. Also, a block-shaped contrast will be analyzed where some integrals can also be determined analytically. A few numerical results will be shown.

I. THEORY

A. Basic acoustic equations

An acoustic medium is considered with constitutive coefficients ρ and κ, where ρ is the volume density of mass, given in $\mathrm{kg\,m^{-3}}$, and κ is the compressibility, given in $\mathrm{Pa^{-1}}$. The wave field in a point of an acoustic medium is fully defined by its pressure p and the three components of the particle velocity v_k. In the medium, two kinds of sources may be present: monopoles and dipoles. A monopole source is described by q, the volume source density of injection rate [1/s]. A dipole source is quantified by f_k, the volume source density of volume force ($\mathrm{N\,m^{-3}}$). In the notation of these quantities and the wave field description, the notation of Fokkema and Van den Berg (1993) is closely followed.

With these quantities, the basic equations describing wave motion are given by Newton's second law, the equation of motion,

$$\partial_k p + \rho\, \partial_t v_k = f_k, \tag{3}$$

and by the deformation equation, using a linear, instantaneously reacting isotropic medium in the low-velocity approximation:

$$\partial_k v_k + \kappa\, \partial_t p = q, \tag{4}$$

where ∂_t stands for differentiation with respect to time, and ∂_k denotes differentiation with respect to the spatial coordinate x_k. The analysis is performed in the Laplace domain, where the Laplace transformation is given by

$$\hat{\phi}(s) = \int_0^\infty \exp(-st)\,\phi(t)\,dt, \tag{5}$$

where ϕ can be any quantity, a hat on top of a quantity denotes that it is in its Laplace-domain representation, and s is the Laplace transform parameter. By applying the one-sided Laplace transformation with respect to time, the above equations are written as

$$\partial_k \hat{p} + s\rho \hat{v}_k = \hat{f}_k \tag{6}$$

and

$$\partial_k \hat{v}_k + s\kappa \hat{p} = \hat{q}, \tag{7}$$

where temporal initial conditions of the wave field are taken into account in the sources.

B. Homogeneous half-space

A homogeneous acoustic half-space is considered. The half-space is of infinite extent in both sides for the x_1 and x_2 directions. The x_3 axis is perpendicular to the bounding surface, and points downward into the half-space. Since there is a contrasting plane, the incident waves will be reflected at the boundary of the half-space, giving rise to a scattered wave field. From Fokkema and Van den Berg (1993), it follows that the total wave field due to a monopole source in a homogeneous acoustic half-space is given by

$$\hat{p}^H(\mathbf{x},s) = \hat{q}^S(s)\hat{G}^H(\mathbf{x}^S|\mathbf{x},s), \tag{8}$$

and

$$\hat{v}_k^H(\mathbf{x},s) = -\hat{q}^S(s)\hat{\Gamma}_k^H(\mathbf{x}^S|\mathbf{x},s). \tag{9}$$

In these expression the Green's functions are introduced for a homogeneous half-space, $\hat{G}^H$ and $\hat{\Gamma}_k^H$, for the pressure and the particle velocity, respectively; the superscript H refers to the half-space, and the superscript S refers to the source position. The Green's functions are given by

$$\hat{G}^H(\mathbf{x}^S|\mathbf{x},s) = \hat{G}(\mathbf{x}-\mathbf{x}^S,s) - \hat{G}(\mathbf{x}-\mathbf{x}^{S*},s) \tag{10}$$

and

$$\hat{\Gamma}_k^H(\mathbf{x}^S|\mathbf{x},s) = \partial_k(\hat{G}(\mathbf{x}-\mathbf{x}^S,s) - \hat{G}(\mathbf{x}-\mathbf{x}^{S*},s)) \tag{11}$$

with $\hat{G}(\mathbf{x},s)$ being defined as:

$$\hat{G}(\mathbf{x},s) = \frac{\exp\left(-\dfrac{s}{c}|\mathbf{x}|\right)}{4\pi|\mathbf{x}|}. \tag{12}$$

S^* is the mirror image of the source position S.

C. Contrasting domain in half-space

Now an acoustic half-space with a contrasting domain, e.g., a geophone-spike, is considered. The total wave field in an acoustic half-space due to a dipole source located somewhere in the medium, but outside a contrasting domain $\partial D_{\mathrm{sct}}$ can be decomposed into two wave fields: an incident wave field and a scattered wave field. The incident field is now considered to be the half-space response. Then, the total pressure is expressed by

$$\hat{p}^{\mathrm{tot}}(\mathbf{x},s) = \hat{p}^H(\mathbf{x},s) + \hat{p}^{\mathrm{sct}}(\mathbf{x},s). \tag{13}$$

In the derivations so far, the expression followed straightforwardly. In this section use is made of the acoustic reciprocity theorem as elaborated in Fokkema and Van den Berg (1993). The acoustic reciprocity theorem is a very elegant way to formulate a scattering problem, especially in geometries of laterally varying structures. In the reciprocity theorem two states are defined for the acoustic source, the material parameters and wave field quantities. In the case of a contrasting domain, the states for the sources are the same, while the states of the material parameters and the wave field quantities are different in the area of the contrasting domain.

Since the incident field is source-free in the contrasting domain, one can write for a point $\mathbf{x}^R$ outside the contrasting domain [Fokkema and Van den Berg, 1993, Eq. (8.46)]:

$$0 = \int_{x\in\partial D_{\mathrm{sct}}} [\hat{G}^H(\mathbf{x}^R|\mathbf{x},s)\hat{v}_k^H(\mathbf{x},s) + \hat{\Gamma}_k^H(\mathbf{x}^R|\mathbf{x},s)\hat{p}^H(\mathbf{x},s)]n_k\,dA, \quad \mathbf{x}^R \in D'_{\mathrm{sct}}. \tag{14}$$

The scattered field is source-free in the domain exterior to the contrasting domain, leading to [Fokkema and Van den Berg, 1993, Eq. (8.47)]

$$\hat{p}^{\mathrm{sct}}(\mathbf{x}^R,s) = \int_{x\in\partial D_{\mathrm{sct}}} [\hat{G}^H(\mathbf{x}^R|\mathbf{x},s)\hat{v}_k^{\mathrm{sct}}(\mathbf{x},s) + \hat{\Gamma}_k^H(\mathbf{x}^R|\mathbf{x},s)\hat{p}^{\mathrm{sct}}(\mathbf{x},s)]n_k\,dA, \quad \mathbf{x}^R \in D'_{\mathrm{sct}}. \tag{15}$$

The scattered field is obtained in terms of the total field by adding Eqs. (14) and (15). However, the goal is to find representations for the limiting behavior where the considered point $\mathbf{x}^R$ approaches the boundary $\partial D_{\mathrm{sct}}$. From Fokkema and Van den Berg's (1993) Eq. (8.56), it follows that the acoustic pressure in a point located at the boundary of the sensor is given by

$$\hat{p}^{\mathrm{sct}}_{\partial D_{\mathrm{sct}}}(\mathbf{x}^R,s)=\tfrac{1}{2}\hat{p}^{\mathrm{tot}}(\mathbf{x}^R,s)+\int_{\mathbf{x}\in\partial D_{\mathrm{sct}}\setminus(\mathbf{x}=\mathbf{x}^R)}[\hat{G}^H(\mathbf{x}^R|\mathbf{x},s)\hat{v}^{\mathrm{tot}}_k(\mathbf{x},s)+\hat{\Gamma}^H_k(\mathbf{x}^R|\mathbf{x},s)\hat{p}^{\mathrm{tot}}(\mathbf{x},s)]n_k\,dA, \tag{16}$$

where integration over the scattering domain now excludes the singular point of observation, which is represented by the term $(1/2)\hat{p}^{\mathrm{tot}}$.

D. Rigid movable object

The condition that the contrast is a movable rigid object will be used now, so the particle velocity is constant in space. Therefore, this particle velocity is denoted with a capital: $\hat{V}^{\mathrm{tot}}_k$. The equation of motion applied to the scattering domain gives

$$\int_{\mathbf{x}\in\partial D}\hat{p}^{\mathrm{tot}}n_k\,dA=-s\hat{V}^{\mathrm{tot}}_k\int_{\mathbf{x}\in D}\rho_{\mathrm{sens}}\,dV \tag{17}$$

in which ρ_{sens} is the density of the sensor. An expression for the pressure $\hat{p}$ as a function of the spatial constant velocity $\hat{V}_k$ is given by

$$\hat{p}^{\mathrm{tot}}=-s\rho_{\mathrm{sens}}x_l\hat{V}^{\mathrm{tot}}_l, \tag{18}$$

which can easily be shown by substituting this solution in Eq. (17) and applying Gauss' divergence theorem. This leads to

$$\hat{V}_l\int_{\mathbf{x}\in D}\partial_k x_l\,dV=\hat{V}_k\int_{\mathbf{x}\in D}dV \tag{19}$$

and the posed solution obeys the equation of motion in global form. So then, for a rigid movable contrast, the scattered field becomes:

$$\hat{p}^{\mathrm{sct}}_{\partial D_{\mathrm{sct}}}(\mathbf{x}^R,s)=\tfrac{1}{2}\hat{p}^{\mathrm{tot}}(\mathbf{x}^R,s)+\hat{V}^{\mathrm{tot}}_k\int_{\mathbf{x}\in\partial D_{\mathrm{sct}}\setminus(\mathbf{x}=\mathbf{x}^R)}\hat{G}^H(\mathbf{x}^R|\mathbf{x},s)n_k\,dA-s\rho_{\mathrm{sens}}\hat{V}^{\mathrm{tot}}_k\int_{\mathbf{x}\in\partial D_{\mathrm{sct}}\setminus(\mathbf{x}=\mathbf{x}^R)}x_k\hat{\Gamma}^H_l(\mathbf{x}^R|\mathbf{x},s)\times n_l\,dA,\quad \mathbf{x}^R\in\partial D'_{\mathrm{sct}}, \tag{20}$$

where now $\hat{V}^{\mathrm{tot}}_k$ is taken outside the integral, since it is a constant along the scattering surface.

E. Coupling coefficients for one-dimensional motion

The goal of this paper is to obtain a coupling coefficient as defined in the introduction, either by $\hat{p}^{\mathrm{tot}}/\hat{p}^H$ or by $\hat{v}^{\mathrm{tot}}_k/\hat{v}^H_k$, where it is understood that the undisturbed state is the field of the half-space, denoted by the superscript H. In order to define the coupling coefficient, $\hat{p}$ needs to be converted to $\hat{v}_k$, or vice versa.

First, the ratio $\hat{p}^{\mathrm{tot}}/\hat{p}^H$ is considered. For this ratio the coefficients v^{tot}_k cannot be determined only in terms of $\hat{p}^{\mathrm{tot}}$, unless a motion only in *one* direction is assumed. Assuming only a motion in the *vertical* direction one can write

$$\hat{v}^{\mathrm{tot}}_3=-\frac{1}{s\rho_{\mathrm{sens}}x_3}\hat{p}^{\mathrm{tot}} \tag{21}$$

as follows from Eq. (18). The scattered field [Eq. (20)] is written as

$$\begin{aligned}\hat{p}^{\mathrm{tot}}(\mathbf{x}^R,s)-\hat{p}^H_{\partial D_{\mathrm{sct}}}(\mathbf{x}^R,s)&=\frac{1}{2}\hat{p}^{\mathrm{tot}}(\mathbf{x}^R,s)-\frac{1}{s\rho_{\mathrm{sens}}x^R_3}\hat{p}^{\mathrm{tot}}(\mathbf{x}^R,s)\times\int_{\mathbf{x}\in\partial D_{\mathrm{sct}}\setminus(\mathbf{x}=\mathbf{x}^R)}\hat{G}^H(\mathbf{x}^R|\mathbf{x},s)n_3\,dA\\&\quad+\frac{1}{x^R_3}\hat{p}^{\mathrm{tot}}(\mathbf{x}^R,s)\int_{\mathbf{x}\in\partial D_{\mathrm{sct}}\setminus(\mathbf{x}=\mathbf{x}^R)}x_3\hat{\Gamma}^H_l(\mathbf{x}^R|\mathbf{x},s)n_l\,dA\\&=B\hat{p}^{\mathrm{tot}}(\mathbf{x}^R,s),\quad \mathbf{x}^R\in D'_{\mathrm{sct}},\end{aligned} \tag{22}$$

where B is the factor which can be determined for any configuration:

$$B=\frac{1}{2}-\frac{1}{s\rho_{\mathrm{sens}}x^R_3}\int_{\mathbf{x}\in\partial D_{\mathrm{sct}}\setminus(\mathbf{x}=\mathbf{x}^R)}\hat{G}^H(\mathbf{x}^R|\mathbf{x},s)n_3\,dA+\frac{1}{x^R_3}\int_{\mathbf{x}\in\partial D_{\mathrm{sct}}\setminus(\mathbf{x}=\mathbf{x}^R)}x_3\hat{\Gamma}^H_l(\mathbf{x}^R|\mathbf{x},s)n_l\,dA. \tag{23}$$

So the interaction coupling coefficient C_I for pressure-sensitive sensors can then be determined as

$$C_I=\frac{\hat{p}^{\mathrm{tot}}}{\hat{p}^H}=\frac{1}{1-B}. \tag{24}$$

This analysis is valid for pressure-sensitive sensors. For sensors sensitive to particle velocity, the equations of motion are used to introduce $\hat{v}^{\mathrm{tot}}_k$, and the scattered field [Eq. (20)] can be written as

$$\begin{aligned}-s\rho_{\mathrm{sens}}x^R_k\hat{v}^{\mathrm{tot}}_k(\mathbf{x}^R,s)+s\rho x^R_k\hat{v}^H_k(\mathbf{x}^R,s)&=-\tfrac{1}{2}s\rho_{\mathrm{sens}}x^R_k\hat{v}^{\mathrm{tot}}_k(\mathbf{x}^R,s)+\hat{v}^{\mathrm{tot}}_k(\mathbf{x}^R,s)\times\int_{\mathbf{x}\in\partial D_{\mathrm{sct}}\setminus(\mathbf{x}=\mathbf{x}^R)}\hat{G}^H(\mathbf{x}^R|\mathbf{x},s)n_l\,dA-s\rho_{\mathrm{sens}}\hat{v}^{\mathrm{tot}}_k(\mathbf{x}^R,s)\\&\quad\times\int_{\mathbf{x}\in\partial D_{\mathrm{sct}}\setminus(\mathbf{x}=\mathbf{x}^R)}x_k\hat{\Gamma}^H_l(\mathbf{x}^R|\mathbf{x},s)n_l\,dA.\end{aligned} \tag{25}$$

Again, the coupling coefficient for each component $\hat{v}_k$ cannot be determined, unless one-dimensional motion is assumed. Again, say that only a motion in the vertical direction exists. Then it holds that

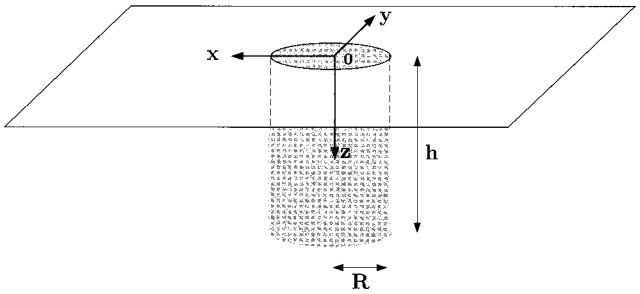

FIG. 1. Configuration for cylinder-shaped contrast.

$$
\begin{aligned}
&-s\rho_{\text{sens}}x_3^R\hat{v}_3^{\text{tot}}(\mathbf{x}^R,s)+s\rho x_3^R\hat{v}_3^H(\mathbf{x}^R,s)\\
&\quad=-s\rho_{\text{sens}}x_3^R\Bigg[\frac{1}{2}+\frac{1}{s\rho_{\text{sens}}x_3^R}\\
&\qquad\times\int_{\mathbf{x}\in\partial D_{\text{sct}}\setminus(\mathbf{x}=\mathbf{x}^R)}\hat{G}^H(\mathbf{x}^R|\mathbf{x},s)n_3\,dA\\
&\qquad+\frac{1}{x_3^R}\int_{\mathbf{x}\in\partial D_{\text{sct}}\setminus(\mathbf{x}=\mathbf{x}^R)}x_3\hat{\Gamma}_l^H(\mathbf{x}^R|\mathbf{x},s)n_l\,dA\Bigg]\hat{v}_3^{\text{tot}}(\mathbf{x}^R,s)\\
&\quad=-s\rho_{\text{sens}}x_3^RB\hat{v}_3^{\text{tot}}(\mathbf{x}^R,s),
\end{aligned}
\tag{26}
$$

where the factor B was as defined before [Eq. (23)]. So the interaction coupling coefficient C_I for velocity-sensitive sensors can be determined as

$$
C_I=\frac{\hat{v}_3^{\text{tot}}}{\hat{v}_3^H}=\frac{\rho}{\rho_{\text{sens}}}\frac{1}{1-B}. \tag{27}
$$

F. Cylindrical contrast

The above expression for the coupling coefficient includes the factor B, which is geometry-dependent. In this section the object is considered as a cylinder, since it resembles the spike of a geophone, which is a velocity-sensitive device. For such an object some of the integrals involved can be determined analytically.

The origin of the coordinate system is chosen as the midpoint of the top of the cylinder. The configuration is given in Fig. 1. The scattering surface ∂D_{sct} is divided into three parts: the top (∂D_{top}), mantle (∂D_{man}), and bottom of the cylinder (∂D_{bot}).

First, the first integral in the expression for B is considered. First, n_3 is zero, thus the product $\hat{v}_3^{\text{tot}}n_3$ is zero at the mantle of the cylinder. Second, the Green's function $\hat{G}^H(\mathbf{x}^R|\mathbf{x},s)$ vanishes at the surface $x_3=0$, which follows from Eq. (A1). The top of the cylinder is assumed to be at the free surface, so this holds for the integral over ∂D_{top}. It follows that

$$
\int_{\mathbf{x}\in\partial D_{\text{sct}}\setminus(\mathbf{x}=\mathbf{x}^R)}\hat{G}^H(\mathbf{x}^R|\mathbf{x},s)n_3\,dA=\int_{\mathbf{x}\in\partial D_{\text{bot}}}\hat{G}^H(\mathbf{x}^R|\mathbf{x},s)dA. \tag{28}
$$

Using Eq. (A1), and considering that at ∂D_{bot}, $x_3=h$, the integral over the bottom of the cylinder can be evaluated analytically:

$$
\begin{aligned}
&\int_{\mathbf{x}\in\partial D_{\text{bot}}\setminus(bfx=\mathbf{x}^R)}\hat{G}^H(\mathbf{x}^R|\mathbf{x},s)dA\\
&\quad=\int_{\theta=0}^{2\pi}\int_{r=0^+}^{R}\frac{s\rho}{4\pi}\Bigg[\frac{\exp\left(-\frac{s}{c}r\right)}{r}\\
&\qquad-\frac{\exp\left(-\frac{s}{c}\sqrt{r^2+4h^2}\right)}{\sqrt{r^2+4h^2}}\Bigg]r\,dr\,d\theta\\
&\quad=\frac{\rho c}{2}\Bigg[-\exp\left(-\frac{s}{c}R\right)+\exp\left(-\frac{s}{c}\sqrt{R^2+4h^2}\right)\\
&\qquad+1-\exp\left(-2\frac{s}{c}h\right)\Bigg].
\end{aligned}
\tag{29}
$$

Next, consider the second integral in the expression for B. Since Γ_3^H is bounded at ∂D_{top}, the integral over the top of the cylinder vanishes since x_3 is zero at the top. At the bottom of the cylinder, $\mathbf{n}$ is given by (0,0,1), and x_3 is constant ($=h$). On the mantle of the cylinder, $\hat{\Gamma}_l^Hn_l$ is given by $\hat{\Gamma}_l^H\cos\theta+\hat{\Gamma}_2^H\sin\theta$. Because of these considerations,

$$
\begin{aligned}
&\int_{\mathbf{x}\in\partial D_{\text{sct}}\setminus(\mathbf{x}=\mathbf{x}^R)}x_3\hat{\Gamma}_l^H(\mathbf{x}^R|\mathbf{x},s)n_l\,dA\\
&\quad=\int_{\mathbf{x}\in\partial D_{\text{man}}}x_3(\hat{\Gamma}_l^H\cos\theta+\hat{\Gamma}_2^H\sin\theta)dA\\
&\qquad+h\int_{\mathbf{x}\in\partial D_{\text{bot}}\setminus(\mathbf{x}-\mathbf{x}^R)}\hat{\Gamma}_3^H(\mathbf{x}^R|\mathbf{x},s)dA.
\end{aligned}
\tag{30}
$$

Now, the integral over the mantle of the cylinder can be written as

$$
\begin{aligned}
\int_{\mathbf{x}\in\partial D_{\text{man}}}x_3\hat{\Gamma}_l^H(\mathbf{x}^R|\mathbf{x},s)n_l\,dA=&-\frac{R^2}{4\pi}\int_{\theta=0}^{2\pi}\int_{x_3=0^+}^{h}x_3\Bigg\{\frac{s}{c}\Bigg[\frac{\exp\left(-\frac{s}{c}\sqrt{R^2+(x_3-h)^2}\right)}{R^2+(x_3-h)^2}-\frac{\exp\left(-\frac{s}{c}\sqrt{R^2+(x_3+h)^2}\right)}{R^2+(x_3+h)^2}\Bigg]\\
&+\frac{\exp\left(-\frac{s}{c}\sqrt{R^2+(x_3-h)^2}\right)}{(R^2+(x_3-h)^2)^{3/2}}-\frac{\exp\left(-\frac{s}{c}\sqrt{R^2+(x_3+h)^2}\right)}{(R^2+(x_3+h)^2)^{3/2}}\Bigg\}dx_3\,d\theta.
\end{aligned}
\tag{31}
$$

Using Eq. (A4), the integral over the bottom of the cylinder can be evaluated analytically:

$$h\int_{\mathbf{x}\in\partial D_{\text{bot}}\setminus(\mathbf{x}-bfx^R)}\hat{\Gamma}_3^H(\mathbf{x}^R|\mathbf{x},s)dA=\frac{h^2}{2\pi}\int_{0=0}^{2\pi}\int_{r=0^+}^{R}\exp\left(-\frac{s}{c}\sqrt{r^2+4h^2}\right)\left[\frac{s}{c}\frac{1}{(r^2+4h^2)}+\frac{1}{(r^2+4h^2)^{3/2}}\right]rd$$

$$=h\frac{\exp\left(-2\frac{s}{c}h\right)}{2}-\frac{h^2}{\sqrt{R^2+4h^2}}\exp\left(-\frac{s}{c}\sqrt{R^2+4h^2}\right). \tag{32}$$

The total expression for B becomes:

$$B=\frac{1}{2}-\frac{1}{s\rho_{\text{sens}}h}\frac{\rho c}{2}\left[-\exp\left(-\frac{s}{c}R\right)+\exp\left(-\frac{s}{c}\sqrt{R^2+4h^2}\right)+1-\exp\left(-2\frac{s}{c}h\right)\right]$$
$$+\frac{\exp\left(-2\frac{s}{c}h\right)}{2}-\frac{h\exp\left(-\frac{s}{c}\sqrt{R^2+4h^2}\right)}{\sqrt{R^2+4h^2}}-\frac{R^2}{2h}\int_{x_3=0}^{h}x_3\left\{\frac{s}{c}\left[\frac{\exp\left(-\frac{s}{c}\sqrt{R^2+(x_3-h)^2}\right)}{R^2+(x_3-h)^2}\right.\right.$$
$$\left.\left.-\frac{\exp\left(-\frac{s}{c}\sqrt{R^2+(x_3+h)^2}\right)}{R^2+(x_3+h)^2}\right]+\frac{\exp\left(-\frac{s}{c}\sqrt{R^2+(x_3-h)^2}\right)}{(R^2+(x_3-h)^2)^{3/2}}-\frac{\exp\left(-\frac{s}{c}\sqrt{R^2+(x_3+h)^2}\right)}{(R^2+(x_3+h)^2)^{3/2}}\right\}dx_3. \tag{33}$$

G. Analytical expression for low frequencies for cylindrical contrast

When the arguments of the exponential functions are smaller than 1, the exponential functions can be approximated by the first few terms of its Taylor expansions. The largest term occurring in the exponential functions is $(s/c)\sqrt{R^2+4h^2}$, so the approximation for the whole expression for B holds for $s<c/\sqrt{R^2+4h^2}$, which means small spikes, or equivalently, low frequencies.

In the expression for B, terms are taken only up to the order s^1. The integrals in B can be determined analytically, using the tables from Gradshteyn and Ryzhik (1980, Tables 2.214.2, 2.145.2, 2.271.4, 2.271.5, 2.271.7):

$$\int_{x_3=0}^{h}x_3\left\{\frac{\exp\left(-\frac{s}{c}\sqrt{R^2+(x_3-h)^2}\right)}{R^2+(x_3-h)^2}-\frac{\exp\left(-\frac{s}{c}\sqrt{R^2+(x_3+h)^2}\right)}{R^2+(x_3+h)^2}\right\}dx_3\approx\frac{1}{2}\ln\left(\frac{R^2}{R^2+4h^2}\right)+\frac{h}{R}\arctan\left(\frac{2h}{R}\right), \tag{34}$$

$$\int_{x_3=0}^{h}x_3\left\{\frac{\exp\left(-\frac{s}{c}\sqrt{R^2+(x_3-h)^2}\right)}{(R^2+(x_3-h)^2)^{3/2}}-\frac{\exp\left(-\frac{s}{c}\sqrt{R^2+(x_3+h)^2}\right)}{(R^2+(x_3+h)^2)^{3/2}}\right\}dx_3$$
$$\approx\left[-\frac{1}{R}+\frac{1}{\sqrt{R^2+4h^2}}+\frac{2h^2}{R^2\sqrt{R^2+4h^2}}\right]+\frac{s}{c}\left[\frac{1}{2}\ln\left(\frac{R^2+4h^2}{R^2}\right)-\frac{h}{R}\arctan\left(\frac{2h}{R}\right)\right]. \tag{35}$$

Using these approximations, the expression for the coupling coefficient for motion-sensitive sensors is obtained:

$$C_I=\frac{\rho 2h\sqrt{R^2+4h^2}}{\rho_{\text{sens}}(R^2+4h^2-R\sqrt{R^2+4h^2})-\rho(R^2+4h^2-(R+2h)\sqrt{R^2+4h^2})}. \tag{36}$$

What can be remarked here is that C_I does not contain any phase factor, and not even any velocity c; notice also that C_I is unity when $\rho=\rho_{\text{sens}}$.

H. Block-shaped contrast

This contrast is chosen because, for seismological stations, sometimes concrete blocks are used for mounting. The procedure as used for the cylindrical contrast will be followed. A full expression for the coupling and an analytical approximation for low frequencies will be given.

The configuration is given in Fig. 2. Again, the point of observation is chosen in the midpoint of the top of the block. The block is divided into the top (∂D_{top}), the sides ($\partial D_{\text{sides}}$), and the bottom ($\partial D_{\text{bot}}$).

First, the first integral in the expression for B is considered. As for the cylinder, the contributions for the top and the sides vanish. As a consequence,

$$\int_{\mathbf{x}\in\partial D_{\mathrm{sct}}\setminus(\mathbf{x}=\mathbf{x}^R)} \hat{G}^H(\mathbf{x}^R|\mathbf{x},s)n_3\,dA$$
$$= \int_{\mathbf{x}\in\partial D_{\mathrm{bot}}} \hat{G}^H(\mathbf{x}^R|\mathbf{x},s)dA$$
$$= \frac{\rho c}{2}\left[1-\exp\left(-\frac{s}{c}2h\right)\right]$$
$$+\frac{2\rho c}{\pi}\int_0^{\pi/4}\left[\exp\left(-\frac{s}{c}\sqrt{d^2+d^2\tan^2\theta+4h^2}\right)\right.$$
$$\left.-\exp\left(-\frac{s}{c}\sqrt{d^2+d^2\tan^2\theta}\right)\right]d\theta. \tag{37}$$

Next, the second integral in the expression for B is considered. The contribution from $\partial D_{\mathrm{top}}$ vanishes since x_3 is zero. It follows that

$$\int_{\mathbf{x}\in\partial D_{\mathrm{sct}}\setminus(\mathbf{x}=\mathbf{x}^R)} x_3\hat{\Gamma}_l^H(\mathbf{x}^R|\mathbf{x},s)n_l\,dA$$
$$= \int_{\mathbf{x}\in\partial D_{\mathrm{sides}}} x_3\hat{\Gamma}_l^H n_l\,dA$$
$$+h\int_{\mathbf{x}\in\partial D_{\mathrm{bot}}\setminus(\mathbf{x}=bfx^R)}\hat{\Gamma}_3^H(\mathbf{x}^R|\mathbf{x},s)dA. \tag{38}$$

The integral over the sides all have the same shape, and add up to give

$$\int_{\mathbf{x}\in\partial D_{\mathrm{sides}}} x_3\hat{\Gamma}_l^H(\mathbf{x}^R|\mathbf{x},s)n_l\,dA = -\frac{2d}{\pi}\int_{x_1=0}^{d}\int_{x_3=0}^{h}x_3\left\{\frac{s}{c}\left[\frac{\exp\left(-\frac{s}{c}\sqrt{r^2+(x_3-h)^2}\right)}{r^2+(x_3-h)^2}-\frac{\exp\left(-\frac{s}{c}\sqrt{r^2+(x_3+h)^2}\right)}{r^2+(x_3+h)^2}\right]\right.$$
$$\left.+\frac{\exp\left(-\frac{s}{c}\sqrt{r^2+(x_3-h)^2}\right)}{(r^2+(x_3-h)^2)^{3/2}}-\frac{\exp\left(-\frac{s}{c}\sqrt{r^2+(x_3+h)^2}\right)}{(r^2+(x_3+h)^2)^{3/2}}\right\}dx_3\,dx_1, \tag{39}$$

in which r is given by $r^2=x_1^2+d^2$. The integral over the bottom becomes:

$$h\int_{\mathbf{x}\in\partial D_{\mathrm{bot}}\setminus(\mathbf{x}=\mathbf{x}^R)}\hat{\Gamma}_3^H(\mathbf{x}^R|\mathbf{x},s)dA$$
$$= \frac{4h^2}{\pi}\int_{\theta=0}^{\pi/4}\int_{r=0^+}^{\sqrt{d^2+d^2\tan^2\theta}}\exp\left(-\frac{s}{c}\sqrt{r^2+4h^2}\right)$$
$$\times\left[\frac{s}{c}\frac{1}{r^2+h^2}+\frac{1}{(r^2+4h^2)^{3/2}}\right]r\,dr\,d\theta$$
$$= \frac{h}{2}\exp\left(-\frac{s}{c}2h\right)$$
$$-\frac{4h^2}{\pi}\int_{\theta=0}^{\pi/4}\frac{\exp\left(-\frac{s}{c}\sqrt{d^2+d^2\tan^2\theta+4h^2}\right)}{\sqrt{d^2+d^2\tan^2\theta+4h^2}}d\theta. \tag{40}$$

With these expressions, the exact total coupling coefficient can be determined as for the cylindrical case.

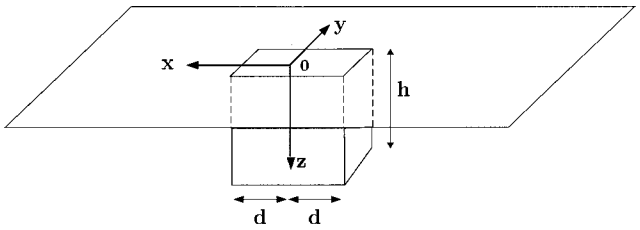

FIG. 2. Configuration for block-shaped contrast.

I. Analytical expression for low frequencies for block-shaped contrast

In the cylindrical case, an analytical expression was derived for low frequencies; in the case of the block, the expressions are more elaborate and therefore the expression has only be determined for $\omega=0$. This means that here it is not shown directly that the first-order term vanishes, although numerically it also showed a negligible small contribution in the first-order (imaginary) term.

The integrals for the block-shaped contrast have again be determined using the tables from Gradshteyn and Ryzhik (1980, Tables 2.271.4, 2.141.2, 2.275.4):

$$\int_{x_1=0}^{d}\int_{z=0}^{h}x_3\left[\frac{1}{(r^2+(x_3-h)^2)^{3/2}}-\frac{1}{(r^2+(x_3+h)^2)^{3/2}}\right]dx_1\,dx_3$$
$$= -\ln\frac{(1+\sqrt{2})(d^2+4h^2)^{1/2}}{(d+\sqrt{2d^2+4h^2})}+\frac{h}{d}\arctan\left(\frac{2h}{\sqrt{2d^2+4h^2}}\right) \tag{41}$$

$$\int_0^{\pi/4}[\sqrt{d^2+d^2\tan^2\theta}-\sqrt{d^2+d^2\tan^2\theta+4h^2}]d\theta$$
$$= +d\ln\frac{(\sqrt{d^2+4h^2})}{(d+\sqrt{2d^2+4h^2})}\frac{(\sqrt{2}+1)^{1/2}}{(\sqrt{2}-1)^{1/2}}-h\pi$$
$$+2h\arctan\left(\frac{\sqrt{2d^2+4h^2}}{2h}\right) \tag{42}$$

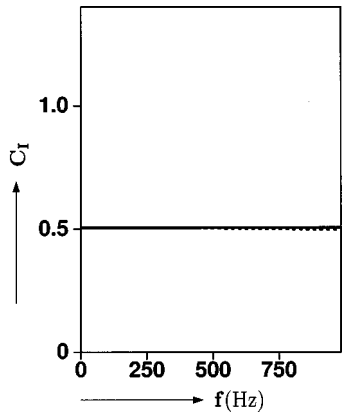

FIG. 3. Velocity-coupling function for cylinder as function of frequency f; $\rho_{\text{sens}}=3000\ \text{kg/m}^3$, $\rho=1500\ \text{kg/m}^3$, $h=0.1$ m, $R=0.005$ m, $c=200$ m/s. Solid line: exact; dashed line: low frequency approximation.

$$\int_0^{\pi/4}\frac{1}{\sqrt{d^2+d^2\tan^2\theta+4h^2}}d\theta = \frac{\pi}{4h}-\frac{1}{2h}\arctan\left(\frac{\sqrt{2d^2+4h^2}}{2h}\right). \tag{43}$$

The total expression for frequency zero then becomes

$$C_I=\frac{\rho}{\rho_{\text{sens}}b_1-\rho b_2}, \tag{44}$$

in which b_1 and b_2 are given by:

$$b_1=1-\frac{2}{\pi}\arctan\left(\frac{d^2}{h\sqrt{2d^2+4h^2}}\right) - \frac{d}{\pi h}\ln\frac{(1+\sqrt{2})^2(d^2+4h^2)}{(d+\sqrt{2d^2+4h^2})^2}, \tag{45}$$

$$b_2=1-\frac{4}{\pi}\arctan\left(\frac{\sqrt{2d^2+4h^2}}{2h}\right) - \frac{d}{\pi h}\ln\frac{(\sqrt{2}+1)}{(\sqrt{2}-1)}\frac{(d^2+4h^2)}{(d+\sqrt{2d^2+4h^2})^2}. \tag{46}$$

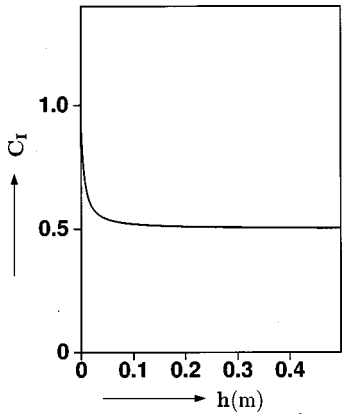

FIG. 4. Velocity-coupling function for cylinder as function of height h; $f=200$ Hz, $\rho_{\text{sens}}=3000\ \text{kg/m}^3$, $\rho=1500\ \text{kg/m}^3$, $R=0.005$ m, $c=200$ m/s. Solid line: exact; dashed line: low frequency approximation.

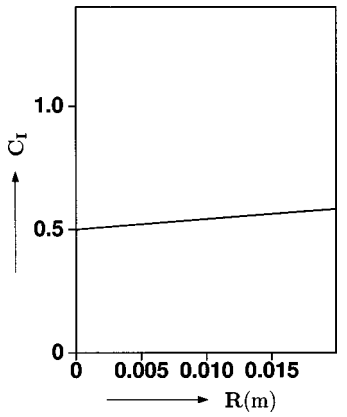

FIG. 5. Velocity-coupling function for cylinder as function of radius R; $f=200$ Hz, $\rho_{\text{sens}}=3000\ \text{kg/m}^3$, $\rho=1500\ \text{kg/m}^3$, $h=0.1$ m, $c=200$ m/s. Solid line: exact; dashed line: low frequency approximation.

II. NUMERICAL RESULTS

In Fig. 3, the velocity-coupling for a cylindrical object is plotted as a function of the frequency. The parameters are chosen for realistic circumstances of geophones as used for land seismics. Both the results of the analytical approximation for low frequencies and the exact representation—the integrals are calculated using a numerical technique—are shown. It is clear that the approximation for low frequencies is useful for these sizes of the sensor, since their values almost coincide on the figures. Also, the coupling is rather insensitive for frequency changes. In this figure, the contrasting domain is rather small. Notice that for the limit to zero frequency, the coupling reaches the value ρ/ρ_{sens}.

In the next two figures, the influence of the geometry of the spike is shown. In Fig. 4 the influence of the height h is shown; the approximation is very good for common values of the geophone dimensions and coincides with the exact value. Notice here that for the limit to zero height, the coupling approaches unity. In Fig. 5, the influence of the radius R on the coupling is shown. Again, the approximation is very good for these parametera and coincides with the exact values; for the limit to zero radius, the coupling approaches ρ/ρ_{sens}.

Geophones are velocity-measuring devices, while hydrophones are pressure-measuring devices. In Fig. 6 the

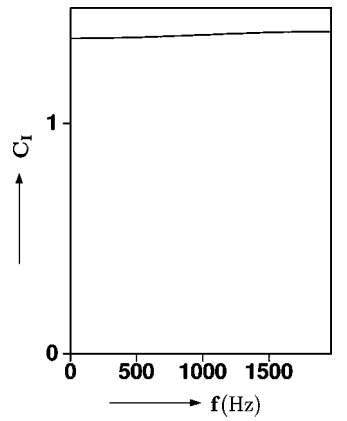

FIG. 6. Pressure-coupling function for cylinder as function of frequency f; $\rho_{\text{sens}}=1500\ \text{kg/m}^3$, $\rho=1000\ \text{kg/m}^3$, $h=0.005$ m, $R=0.025$ m, $c=1500$/s.

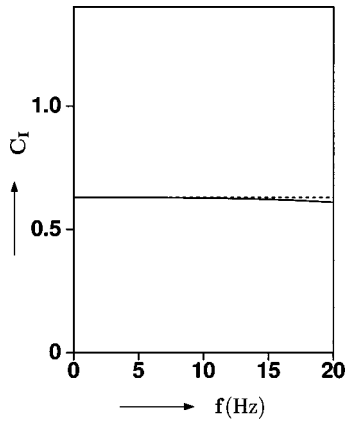

FIG. 7. Velocity-coupling function for block as function of frequency f; $\rho_{sens}=3000\ \mathrm{kg/m^3}$, $\rho=1500\ \mathrm{kg/m^3}$, $h=1$ m, $d=1$ m, $c=200$ m/s. Solid line: exact; dashed line: low frequency approximation.

pressure-coupling for a hydrophone is shown as a function of the frequency. It turns out that this coupling is not very dependent on the frequency. In the next figures, the velocity-coupling for a blocked shape with larger dimensions and using lower frequencies is calculated. The values here are chosen for realistic circumstances of seismological stations as used in seismology. From Fig. 7, it follows that the low frequency approximation is very good again for these sizes of the block. Again, the coupling does not vary much as a function of the frequency. In Figs. 8 and 9, the influence of the geometry is shown. The same behavior as for the cylinder is observed. Geometry factors do have a larger influence on large objects than on small objects. A better coupling is achieved when using thin blocks with large horizontal dimensions.

III. DISCUSSION

In the results, it can be seen that the dominant effect is the density effect; if there is no density contrast, the coupling coefficient is unity. However, it should be realized that the density contrast has arisen because the point of observation is *on* the scattering object and the density has been chosen to be the density of the sensor [see Eq. (17)]. It is arguable whether this density should be the average between the density of the sensor and that of the surrounding medium. In that case, the coupling coefficient would be different in their density term.

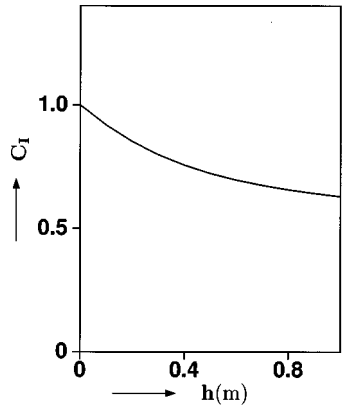

FIG. 8. Velocity-coupling function for block as function of height h; $f=2.5$ Hz, $\rho_{sens}=3000\ \mathrm{kg/m^3}$, $\rho=1500\ \mathrm{kg/m^3}$, $d=1$ m, $c=200$ m/s.

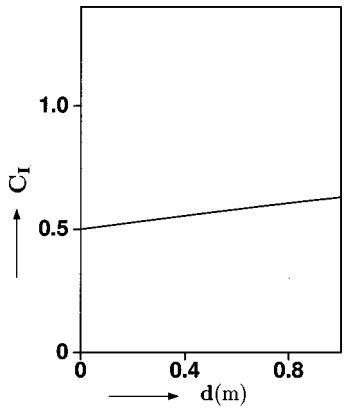

FIG. 9. Velocity-coupling function for block as function of width d; $f=2.5$ Hz, $\rho_{sens}=3000\ \mathrm{kg/m^3}$, $\rho=1500\ \mathrm{kg/m^3}$, $h=1$ m, $c=200$ m/s.

The approach in this paper is that a welded contact between the sensor and the surrounding medium is assumed. In practice, it often occurs that the coupling is not good, and then the model developed here does not account for it. One approach would be to introduce slip along the sensor, by introducing a linear-slip model along the sensor, or by introducing a small ''boundary layer'' which has damping effects. This will be part of future studies.

IV. CONCLUSIONS

In this paper, a general approach for describing the disturbance of a wave field due to the presence of a measuring device has been developed. It was shown that, even when there is perfect material contact between the device and its environment, the measured wave field differs from the wave field that would exists if no measuring device was present. This effect is called the interaction coupling.

The interaction coupling is mainly dependent on the densities of the materials of the measuring device and the surroundings, and on the geometric dimensions of the device. The frequency spectrum of the waves is only of minor importance, as was shown via the low frequency approximations. These low frequency approximations clearly show the main physics of interaction coupling.

APPENDIX: GREEN'S FUNCTIONS FOR CYLINDRICAL OBJECT

In this Appendix explicit expressions are given for the Green's functions $\hat{G}^H$ and $\hat{\Gamma}_k^H$ for the half-space which are needed for evaluating the interaction coupling. The contrasting domain is considered as a cylinder, so it is advantageous to turn to cylindrical coordinates. The cylinder is vertically planted and with its upper plane equal to the surface of the earth. The middle of the cylinder's upper plane is taken to be the origin of a cylindrical coordinate system. The x_3-axis is pointing downward. Use will be made of Eq. (16), where the fixed point x^R has to be located on the boundary of the cylinder. For this reason, the fixed point is taken to be the middle point of the cylinder's lower plane.

The Green's function $\hat{G}^H$ becomes:

$$\hat{G}^H(\mathbf{x}^R|\mathbf{x},s)=\frac{s\rho}{4\pi}\left[\frac{\exp\left(-\frac{s}{c}\sqrt{r^2+(x_3-h)^2}\right)}{\sqrt{r^2+(x_3-h)^2}}-\frac{\exp\left(-\frac{s}{c}\sqrt{r^2+(x_3+h)^2}\right)}{\sqrt{r^2+(x_3+h)^2}}\right], \tag{A1}$$

while the Green's function $\hat{\Gamma}_k^H$ is given by

$$\hat{\Gamma}_1^H(\mathbf{x}^R|\mathbf{x},s)=-\frac{r\cos\theta}{4\pi}\left\{\frac{s}{c}\left[\frac{\exp\left(-\frac{s}{c}\sqrt{r^2+(x_3-h)^2}\right)}{r^2+(x_3-h)^2}-\frac{\exp\left(-\frac{s}{c}\sqrt{r^2+(x_3+h)^2}\right)}{r^2+(x_3+h)^2}\right]\right.$$
$$\left.+\frac{\exp\left(-\frac{s}{c}\sqrt{r^2+(x_3-h)^2}\right)}{(r^2+(x_3-h)^2)^{3/2}}-\frac{\exp\left(-\frac{s}{c}\sqrt{r^2+(x_3+h)^2}\right)}{(r^2+(x_3+h)^2)^{3/2}}\right\}, \tag{A2}$$

$$\hat{\Gamma}_2^H(\mathbf{x}^R|\mathbf{x},s)=-\frac{r\sin\theta}{4\pi}\left\{\frac{s}{c}\left[\frac{\exp\left(-\frac{s}{c}\sqrt{r^2+(x_3-h)^2}\right)}{r^2+(x_3-h)^2}-\frac{\exp\left(-\frac{s}{c}\sqrt{r^2+(x_3+h)^2}\right)}{r^2+(x_3+h)^2}\right]\right.$$
$$\left.+\frac{\exp\left(-\frac{s}{c}\sqrt{r^2+(x_3-h)^2}\right)}{(r^2+(x_3-h)^2)^{3/2}}-\frac{\exp\left(-\frac{s}{c}\sqrt{x^2+(x_3+h)^2}\right)}{(r^2+(x_3+h)^2)^{3/2}}\right\}, \tag{A3}$$

$$\hat{\Gamma}_3^H(\mathbf{x}^R|\mathbf{x},s)=-\frac{1}{4\pi}\left\{\frac{s}{c}\left[\frac{(x_3-h)\exp\left(-\frac{s}{c}\sqrt{r^2+(x_3-h)^2}\right)}{r^2+(x_3-h)^2}-\frac{(x_3+h)\exp\left(-\frac{s}{c}\sqrt{r^2+(x_3+h)^2}\right)}{r^2+(x_3+h)^2}\right]\right.$$
$$\left.+\frac{(x_3-h)\exp\left(-\frac{s}{c}\sqrt{r^2+(x_3-h)^2}\right)}{(r^2+(x_3-h)^2)^{3/2}}-\frac{(x_3+h)\exp\left(-\frac{s}{c}\sqrt{r^2+(x_3+h)^2}\right)}{(r^2+(x_3+h)^2)^{3/2}}\right\}, \tag{A4}$$

where the following relation has been used:

$$\hat{\Gamma}_k^H(x^R|x,s)=\frac{1}{s\rho}\,\partial_k\hat{G}^H(x^R|x,s). \tag{A5}$$

Fokkema, J. T., and van den Berg, P. M. (**1993**). *Seismic Applications of the Acoustic Reciprocity Theorem* (Elsevier, Amsterdam).

Gradshteyn, I. S., and Ryzhik, I. M. (**1980**). *Table of Integrals, Series and Products* (Academic, Orlando, FL).

Tan, T. H. (**1987**). ''Reciprocity theorem applied to the geophone-ground coupling problem,'' Geophysics **52**, 1715–1717.